Available online at www.sciencedirect.com
SCIENCE DIRECT®
ELSEVIER
Nuclear Instruments and Methods in Physics Research B 230 (2005) 142–147
NIM B
Beam Interactions with Materials & Atoms
www.elsevier.com/locate/nimb

Dynamic interactions of fast ions with carbon nanotubes

D.J. Mowbray [a], Sangwoo Chung [a], Z.L. Mišković [a,*], F.O. Goodman [a], You-Nian Wang [b]

[a] *Department of Applied Mathematics, University of Waterloo, 200 University Avenue, Waterloo, Ontario, Canada N2L 3G1*
[b] *The State Key Laboratory of Materials Modification by Beams, Department of Physics, Dalian University of Technology, Dalian 116023, PR China*

Available online 21 January 2005

Abstract

We used the hydrodynamic model to describe the dielectric response of a multi-walled carbon nanotube to a fast point charge moving paraxially, either inside or outside the nanotube. Calculations are performed for a two-walled nanotube, giving rise to a splitting of the plasmon frequencies due to the interaction between the electron fluids on the two cylinders. The dependences of the projectile stopping power and the self-energy (image potential) on the velocity and the distance from the nanotube axis show interesting features when the projectile velocity matches the phase velocity of the plasmon mode with a quasi-linear dispersion.

PACS: 79.20.Rf; 34.50.Bw; 34.50.Dy
Keywords: Carbon nanotube; Plasmon excitation; Stopping power; Self-energy

1. Introduction

The dielectric response properties of carbon nanotubes have been studied extensively in the past several years, both experimentally [1] and theoretically [2–9]. These properties play important role in, e.g. the electron energy loss spectroscopy (EELS) [6,7], and the screening of charged impurities in carbon nanotubes [8]. In addition, there are several, very interesting, recent studies of the charge–particle interactions with nanotubes, namely, the transport of ion or electron beams through the nanotubes [10–14], and the formation of toroidal electron image states around nanotubes [15,16], which would benefit from a detailed theoretical account of the nanotube dielectric response.

On the theoretical side, Arista and coworkers have used the dielectric response formalism in the cylindrical geometry to study the channeling

* Corresponding author. Tel.: +1 519 888 4567; fax: +1 519 746 4319.
E-mail address: zmiskovi@math.uwaterloo.ca (Z.L. Mišković).

0168-583X/$ - see front matter © 2005 Elsevier B.V. All rights reserved.
doi:10.1016/j.nimb.2004.12.032

of fast ions through nanocapillaries in solids [17,18] and the plasmon excitations in cylindrical nanowires by external charged particles [19]. A similar approach has been used recently to evaluate the stopping power and the self-energy (or the image potential) of fast ions moving inside the cylindrical tubules [20], based on the dielectric function in random-phase approximation (RPA) [2]. However, for the dynamical interactions involving plasmon excitations in many-electron systems, one of the most convenient formulations of the dielectric properties in restricted geometries is based on the hydrodynamic model [4–6,21,22]. The simplest version of this model, applicable to carbon nanotubes, assumes that the electrons form a two-dimensional (2D) charged fluid confined to the cylindrical surface of a nanotube wall. Such a model has been used to calculate the plasmon spectra in multi-walled nanotubes (MWNT) [4], and to evaluate the energy losses of charged particles moving perpendicularly to a single-walled nanotube (SWNT) [6], as well as the self-energy and the stopping power of particles moving paraxially inside a SWNT [21]. In particular, it was shown in [21] that the results from the 2D hydrodynamic model agree very well with those obtained from the dielectric-response formalism in RPA [2,20] for fast ions or electrons moving paraxially through a SWNT.

It is well known that layered materials, such as superlattices or layered films, exhibit very rich spectra of collective, or plasmon excitations [23,24]. This is also true for curved geometries at the nanoscale, such as, e.g. multiple metallic nanoshells [22] and MWNT [4]. Since the plasmon excitations play the dominant role in screening and energy losses of external charges, we explore in the present contribution how the splitting of plasmon dispersions in a two-walled nanotube (2WNT) affects the stopping power and the self-energy of a fast point charge moving inside or outside the nanotube, parallel to its axis. We use the hydrodynamic model, in which the 2WNT is represented by two infinitely long concentric cylinders, each containing a 2D charged fluid, so that the electrostatic interaction between those fluids gives rise to a splitting in the plasmon spectrum.

Atomic units (a.u.) are used throughout, unless otherwise indicated.

2. Basic theory

The model is formulated for the general case of a MWNT consisting of N concentric cylinders with radii $a_1 < a_2 < \cdots < a_N$, each occupied by a 2D electron fluid with the equilibrium number density per unit area of $n_0 = 0.428$ corresponding to four valence electrons per carbon atom. We use cylindrical coordinates $\mathbf{x} = \{r, \varphi, z\}$ for an arbitrary point in space, and define $\mathbf{x}_j = \{a_j, \varphi, z\}$ to represent the coordinates of a point on the cylindrical surface $r = a_j$ of the jth nanotube. Similarly, $\nabla_j = \hat{\mathbf{e}}_z \frac{\partial}{\partial z} + a_j^{-1} \hat{\mathbf{e}}_\varphi \frac{\partial}{\partial \varphi}$ differentiates only tangentially to the surface of the jth nanotube. Let the perturbed state of the electron fluid on the jth nanotube be described by the electron number density per unit area, $n_0 + n_j(\mathbf{x}_j, t)$, and by the velocity field, $\mathbf{u}_j(\mathbf{x}_j, t)$, which only has components tangential to the nanotube surface $r = a_j$. Assuming that the system is perturbed by a weak external potential $\Phi_{\text{ext}}(\mathbf{x}, t)$, we obtain, for each j, the linearized continuity equation for the induced density n_j,

$$\frac{\partial n_j(\mathbf{x}_j, t)}{\partial t} + n_0 \nabla_j \cdot \mathbf{u}_j(\mathbf{x}_j, t) = 0 \tag{1}$$

and the linearized momentum-balance equation,

$$\frac{\partial \mathbf{u}_j(\mathbf{x}_j, t)}{\partial t} = \nabla_j \Phi(\mathbf{x}, t)|_{r=a_j} - \frac{\alpha}{n_0} \nabla_j n_j(\mathbf{x}_j, t) + \frac{\beta}{n_0} \nabla_j \left[\nabla_j^2 n_j(\mathbf{x}_j, t) \right] - \gamma \mathbf{u}_j(\mathbf{x}_j, t). \tag{2}$$

The first term on the right-hand-side of Eq. (2) is the force on an electron due to the tangential component of the total electric field, evaluated at the nanotube surface $r = a_j$. In order to obtain the total electric potential, $\Phi = \Phi_{\text{ext}} + \Phi_{\text{ind}}$, we solve the 3D Poisson equation in free space [21], so that the induced potential due to the perturbations of the electron fluid densities on all nanotube surfaces can be simply written as

$$\Phi_{\text{ind}}(\mathbf{x}, t) = -\sum_l \int \mathrm{d}^2 \mathbf{x}'_l \frac{n_l(\mathbf{x}'_l, t)}{\|\mathbf{x} - \mathbf{x}'_l\|}, \tag{3}$$

where $\mathbf{x}'_l = \{a_l, \varphi', z'\}$ while $\mathrm{d}^2\mathbf{x}'_l = a_l \mathrm{d}\varphi' \mathrm{d}z'$ is the differential surface element on the lth nanotube. Note that writing the explicit solution of the Poisson equation provides a more direct approach to solving Eqs. (1) and (2) than the usual method based on undetermined coefficients [4,6,21], because Eq. (3) guarantees that the boundary conditions at all surfaces $r = a_j$ are automatically satisfied. The second term on the right-hand-side of Eq. (2) is the force due to the internal interactions in the jth electron fluid, with $\alpha = \pi n_0$ being the square of the speed of propagation of the density disturbances in a 2D Fermi electron gas [6], whereas the third term with $\beta = 1/4$ comes from the quantum correction for the kinetic energy in this gas and, as such, describes the onset of single-electron excitations in the fluid [21]. The last term in Eq. (2) represents the frictional force on an electron due to the scattering on the positive-charge background, with γ being the friction coefficient, which we take here as a vanishingly small parameter.

We define the Fourier–Bessel (FB) transform $\widetilde{A}(m,k,\omega)$ of an arbitrary function $A(\varphi,z,t)$ by

$$A(\varphi,z,t) = \sum_{m=-\infty}^{\infty} \int_{-\infty}^{\infty} \frac{\mathrm{d}k}{(2\pi)^2} \times \int_{-\infty}^{\infty} \frac{\mathrm{d}\omega}{2\pi} \mathrm{e}^{\mathrm{i}kz+\mathrm{i}m\varphi-\mathrm{i}\omega t} \widetilde{A}(m,k,\omega) \tag{4}$$

and apply it to Eqs. (1)–(3), while using the well-known expansion of the Coulomb potential in cylindrical coordinates,

$$\frac{1}{\|\mathbf{x}-\mathbf{x}'\|} = \sum_{m=-\infty}^{\infty} \int_{-\infty}^{\infty} \frac{\mathrm{d}k}{(2\pi)^2} \mathrm{e}^{\mathrm{i}k(z-z')+\mathrm{i}m(\varphi-\varphi')} g(r,r';m,k), \tag{5}$$

where $g(r,r';m,k) \equiv 4\pi I_m(|k|r_<)K_m(|k|r_>)$ with $r_< = \min(r,r')$ and $r_> = \max(r,r')$ and I_m and K_m being the cylindrical Bessel functions of integer order m. As a result, we can express the FB transform of the induced potential as follows

$$\tilde{\Phi}_{\mathrm{ind}}(r,m,k,\omega) = -\sum_j g(r,a_j;m,k) a_j \tilde{n}_j(m,k,\omega), \tag{6}$$

whereas the FB transforms of the individual induced densities, $\tilde{n}_j(m,k,\omega)$, are obtained by solving the N coupled linear equations,

$$\left[\omega(\omega+\mathrm{i}\gamma) - \alpha\left(k^2+\frac{m^2}{a_j^2}\right) - \beta\left(k^2+\frac{m^2}{a_j^2}\right)^2\right] \times \tilde{n}_j(m,k,\omega) - \sum_l G_{jl}(m,k)\tilde{n}_l(m,k,\omega) = -n_0\left(k^2+\frac{m^2}{a_j^2}\right)\tilde{\Phi}_{\mathrm{ext}}(a_j,m,k,\omega), \tag{7}$$

where $G_{jl}(m,k) \equiv n_0 a_l (k^2 + \frac{m^2}{a_j^2}) g(a_j,a_l;m,k)$. Note that, upon setting $\alpha = 0$, $\beta = 0$, $\gamma = 0$, and $\Phi_{\mathrm{ext}} = 0$ in Eq. (7), those equations become identical to the eigen-frequency equation [4, Eq. (13)] for the resonant plasmon frequencies of a MWNT.

While Eq. (7) with $j = 1, 2, \ldots, N$ can be used to study the interactions of a charged particle with a MWNT made of N concentric cylinders, we limit our attention to 2WNT with two cylinders, $N = 2$. In this case, the resulting 2×2 matrix on the left-hand-side of Eq. (7) gives the eigenvalue equation for the resonant frequencies of the collective excitations in the coupled 2D fluids, with the following two branches of the dispersion relations for each m,

$$\omega_\pm^2 = \frac{\omega_1^2+\omega_2^2}{2} \pm \sqrt{\left(\frac{\omega_1^2-\omega_2^2}{2}\right)^2 + \Delta^2}, \tag{8}$$

where $\omega_j^2 = \pi n_0(k^2+m^2/a_j^2) + \frac{1}{4}(k^2+m^2/a_j^2)^2 + n_0 a_j (k^2+m^2/a_j^2) g(a_j,a_j;m,k)$ are the (squares of the) resonant frequencies of the individual electron fluids on the cylinders $j = 1$ and 2 [21], whereas $\Delta^2 = n_0^2 a_1 a_2 (k^2+m^2/a_1^2)(k^2+m^2/a_2^2) g^2(a_1,a_2;m,k)$ describes the electrostatic interaction between the two fluids.

3. Results

As an example, we choose a 2WNT with the inner and outer cylinders having radii $a_1 = 6.80 = 3.6$ Å and $a_2 = 13.23 = 7$ Å, respectively, with $d = a_2 - a_1 = 6.43 = 3.4$ Å chosen to match the typical inter-wall distance in MWNTs. In Fig. 1 we show the two groups of the resonant plasmon dispersions from Eq. (8), $\omega_+(m,k)$ and $\omega_-(m,k)$, versus the longitudinal wavevector k and for several angular modes $m = 0, 1, 2, 3$ and 4. It is apparent in Fig. 1 that the splitting between

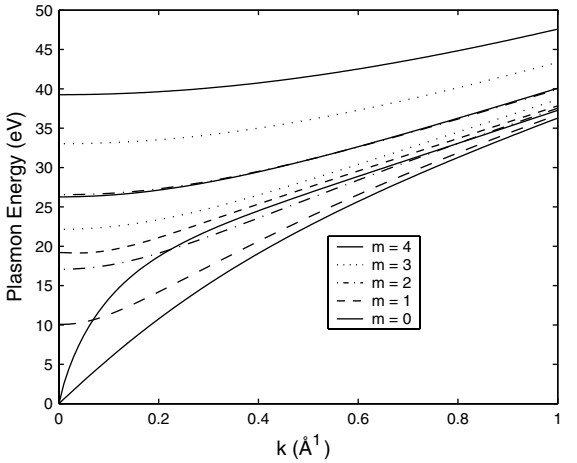

Fig. 1. Plasmon eigen-frequencies (in eV) versus longitudinal wavenumber k (in Å^{-1}) in a two-walled carbon nanotube with radii $a_1 = 6.80$ and $a_2 = 13.23$ a.u. are shown for several angular modes m, labeled by different line-styles, as indicated in the legend. For each m, the upper and lower curve, drawn with the same line-style, correspond to the plasmon dispersion $\omega_+(m,k)$ and $\omega_-(m,k)$ from Eq. (8), respectively.

the two groups of plasmon frequencies in Eq. (8) is rather substantial owing to the strong electrostatic interaction between the two charged fluids. While the upper group of plasmon dispersions exhibits a characteristic dimensional cross-over from a 2D to a one-dimensional electron system [2,4], the lower group of the plasmon frequencies exhibits weaker dispersions with less spreading among various m-modes. In particular, the $m = 0$ mode in the lower-energy plasmon group exhibits a quasi-linear dispersion in the limit of long wavelengths, which can be derived analytically in the form $\omega_-(0,k) \approx v_p k$, with the phase velocity $v_p = \sqrt{4\pi n_0 [a_1 a_2/(a_1 + a_2)] \ln(a_2/a_1)} \approx 4$. This quasi-acoustic plasmon mode seems to be a common occurrence when a splitting of plasmon frequencies happens due to the electrostatic interaction, e.g. in the electron–hole plasma of a carbon nanotube [3], or in the coupling between two parallel nanotubes [9].

We further study the stopping power S for a point charge $Q = 1$ (proton) moving parallel to the axis of the 2WNT on a trajectory $\mathbf{x}_0(t) = \{r_0, \varphi_0, vt\}$, so that $\tilde{\Phi}_{\rm ext}(r,m,k,\omega) = 2\pi g(r,r_0;m,k)\delta(\omega - kv)\exp(-{\rm i}m\varphi_0)$. The calculations in the remainder of this section are performed with the friction coefficient $\gamma = 10^{-3}\Omega_p$, where $\Omega_p = \sqrt{4\pi n_0/a_1}$. Using the definition $S = Q\partial\Phi_{\rm ind}/\partial z|_{\mathbf{x}=\mathbf{x}_0(t)}$, we calculate the velocity dependence of the stopping power for a particle moving along the axis ($r_0 = 0$) of the 2WNT, and show the results in Fig. 2. For the sake of comparison, also shown in Fig. 2 are the stopping powers for two cases of a particle moving along the axis of one-cylinder nanotubes, having the radii $a = 6.80$ and 13.23. It should be noted that only the $m = 0$ plasmon modes can contribute to the energy losses in the case $r_0 = 0$. Clearly, there exists an overall threshold of $v \approx 2$ for the plasmon excitation. While the one-cylinder cases show the characteristic, broadly peaked structures seen earlier [20,21], the stopping in the two-cylinder nanotube shows some novel structure around $v \approx 4$ in the form of a relatively narrow peak superimposed on the low-velocity slope of a broad structure. This broad structure takes intermediate values between the two single-cylinder cases at the intermediate velocities, but clearly surpasses them both at higher speeds, indicating a strong positive interference, or the in-phase motion of the two fluids on 2WNT. On the other hand, the narrow peak at around $v = 4$ is likely a consequence of a large-amplitude, out-of-phase motion of those fluids

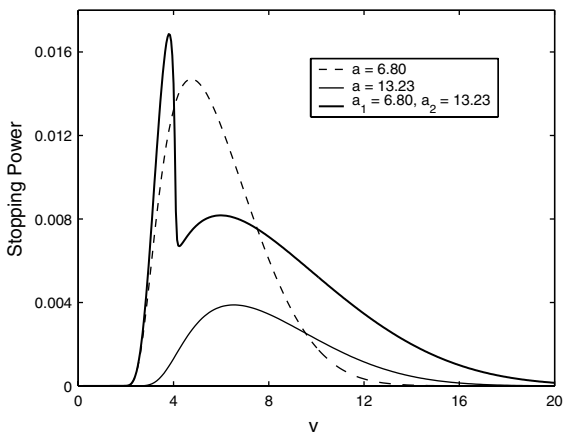

Fig. 2. Stopping power (in a.u.) versus the speed v (in a.u.) for a proton moving along the axis of a nanotube with: two cylinders of radii $a_1 = 6.80$ and $a_2 = 13.23$ a.u. (thick solid line), one cylinder of radius $a = 13.23$ a.u. (thin solid line) and one cylinder of radius $a = 6.80$ a.u. (dotted line).

[3,9], which is triggered by the close matching of the projectile speed and the phase velocity of the quasi-linear, lower $m = 0$ plasmon mode in Fig. 1. This resonant increase of the energy deposition into the collective excitation modes indicates the onset of a possible drift instability of the charged fluids on a 2WNT [9].

Next, we study the situations where the projectile still moves parallel to the nanotube axis, but at finite radial distances, namely, $r_0 = a_1 - d/2 = 3.59 = 1.9$ Å (inside the inner cylinder), $r_0 = (a_1 + a_2)/2 = 10.02 = 5.3$ Å (midway between the two cylindrical surfaces), and $r_0 = a_2 + d/2 = 16.45 = 8.7$ Å (outside the outer cylinder), so that it always stays at the fixed distance $d/2 = 3.21 = 1.7$ Å from the nearest wall(s) of the 2WNT. In such cases, all m-modes contribute to the plasmon excitations. The results for stopping powers in those three cases are shown in Fig. 3, indicating that the narrowly-peaked structure at $v \approx 4$ has been partly merged into the broad structures in the cases of the particle traveling inside or outside the nanotube, whereas the particle moving in between the two cylindrical surfaces shows the most massive energy losses with the narrow peak completely disappeared, or immersed into the broad structure.

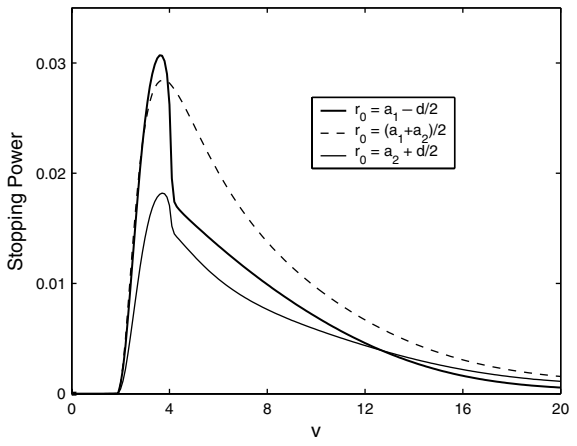

Fig. 3. Stopping power (in a.u.) versus the speed v (in a.u.) for a proton moving parallel to the axis of a nanotube with two cylinders of radii $a_1 = 6.80$ and $a_2 = 13.23$ a.u. at the radial distances: $r_0 = a_1 - d/2$ (thick solid line), $r_0 = a_2 + d/2$ (thin solid line) and $r_0 = (a_1 + a_2)/2$ (dotted line), where $d = a_2 - a_1 = 6.43$ a.u.

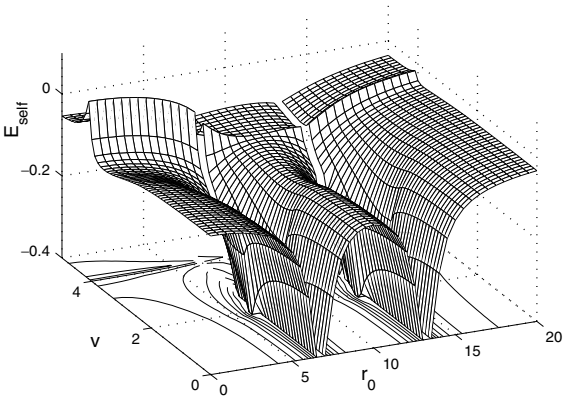

Fig. 4. Self-energy (image potential, in a.u.) versus the speed v (in a.u.) and the radial distances r_0 (in a.u.), for a proton moving parallel to the axis of a nanotube with two cylinders of radii $a_1 = 6.80$ and $a_2 = 13.23$ a.u.

Finally, we calculate the self-energy, or image potential, experienced by a point charge $Q = 1$ at the trajectory $\mathbf{x}_0(t) = \{r_0, \varphi_0, vt\}$, which is defined by $E_{\text{self}} = -\frac{1}{2} Q \Phi_{\text{ind}}|_{\mathbf{x}=\mathbf{x}_0(t)}$. The dependence of the self-energy on the projectile velocity v and the radial distance r_0 from the axis of the 2WNT is shown in Fig. 4, clearly exhibiting attractive wells close to the surfaces of each of the two cylinders, which become shallower with increasing projectile speed. An intriguing ridge in the self-energy occurs for all radial distances (except midway between the two cylinders), at a speed of around $v = 4$, which is clearly in correlation with the onset of a drift instability seen in the stopping powers in Figs. 2 and 3.

4. Concluding remarks

We have formulated a hydrodynamic model for the dielectric response of a MWNT, represented by the set of concentric cylindrical surfaces, each occupied by a 2D electron fluid. Calculations have been completed for a two-cylinder nanotube, showing that the strong electrostatic interaction among the two fluids on these cylinders gives rise to splitting of the collective-excitation frequencies into two sets for various angular modes m, with the lower $m = 0$ mode exhibiting a quasi-acoustic, linear dispersion versus the longitudinal wavenumber k. Calculations of the stopping power for a

charged particle, which moves at speed v, parallel to the nanotube axis at the radial distances inside, outside, or in between the two cylinders, show the typical broad peaks above the plasmon-excitation threshold velocity of about $v = 2$, as well as a narrow peak at about $v = 4$, matching the phase velocity of the quasi-acoustic low-energy plasmon. Calculations of the self-energy of a charged particle moving paraxially show the typical long-ranged attractive wells for the radial distances close to the cylinder walls, which diminish with increasing speed v, with an intriguing jump in the self-energy across the speed $v \approx 4$ for all radial distances. These findings indicate that richness in the plasmon dispersions of MWNT may exert a profound influence on the dynamics of the charged-particle interactions with MWNTs, especially when conditions are met for a drift instability of the electron fluids.

Acknowledgements

This work was supported by the Natural Sciences and Engineering Research Council of Canada. Z.L.M. also acknowledges the support by PREA. Y.-N.W. acknowledges support by the National Natural Science Foundation of China.

References

[1] T. Pichler, M. Knupfer, M.S. Golden, J. Fink, A. Rinzler, R.E. Smalley, Phys. Rev. Lett. 80 (1998) 4729.
[2] M.F. Lin, K.W.-K. Shung, Phys. Rev. B 47 (1993) 6617.
[3] O. Sato, M. Kobayashi, Y. Tanaka, A. Hasegawa, Phys. Rev. B 52 (1995) 4677.
[4] C. Yannouleas, E.N. Bogachek, U. Landman, Phys. Rev. B 53 (1996) 10225.
[5] B. Vasvári, Phys. Rev. B 55 (1997) 7993.
[6] T. Stöckli, J.M. Bonard, A. Châtelain, Z.L. Wang, P. Stadelmann, Phys. Rev. B 64 (2001) 115424.
[7] D. Taverna, M. Kociak, V. Charbois, L. Henrard, Phys. Rev. B 66 (2002) 235419.
[8] K. Sasaki, Phys. Rev. B 65 (2002) 195412.
[9] G. Gumbs, A. Balassis, Phys. Rev. B 68 (2003) 075405.
[10] L.A. Gevorgian, K.A. Ispirian, R.K. Ispirian, Nucl. Instr. and Meth. B 145 (1998) 155.
[11] G.V. Dedkov, B.S. Karamurzov, Surf. Coat. Technol. 128–129 (2000) 51.
[12] N.K. Zhevago, V.I. Glebov, Phys. Lett. A 310 (2003) 301.
[13] S. Bellucci, V.M. Biryukov, Yu.A. Chesnokov, V. Guidi, W. Scandale, Nucl. Instr. and Meth. B 202 (2003) 236.
[14] A.A. Greenenko, N.F. Shul'ga, Nucl. Instr. and Meth. B 205 (2003) 767.
[15] B.E. Granger, P. Král, H.R. Sadeghpour, M. Shapiro, Phys. Rev. Lett. 89 (2002) 135506.
[16] D. Segal, P. Král, M. Shapiro, Phys. Rev. B 69 (2004) 153405.
[17] N.R. Arista, M.A. Fuentes, Phys. Rev. B 63 (2001) 165401.
[18] N.R. Arista, Phys. Rev. A 64 (2001) 032901.
[19] J.L. Gervasoni, N.R. Arista, Phys. Rev. B 68 (2003) 235302.
[20] Y.-N. Wang, Z.L. Mišković, Phys. Rev. A 66 (2002) 042904.
[21] Y.N. Wang, Z.L. Mišković, Phys. Rev. A 69 (2004) 022901.
[22] E. Prodan, P. Nordlander, J. Chem. Phys. 120 (2004) 5444.
[23] G.F. Giuliani, J.J. Quinn, Phys. Rev. Lett. 51 (1983) 919.
[24] J.K. Jain, P.B. Allen, Phys. Rev. Lett. 54 (1985) 2437.